Proceedings of the
Annual Stability Conference
Structural Stability Research Council
Louisville, Kentucky, April 1-4, 2025

Strategic Use of Austenitic Stainless Steel in Dissipative Zones of Eccentrically Braced Frames

Lucy Lázaro[1], Rolando Chacón[2]

Abstract

Stainless steel is a highly durable material known for its high levels of ductility and strain hardening properties. These characteristics make it particularly attractive in applications where material deformation and energy dissipation are critical, such as in seismic design. Austenitic stainless steel, specifically EN 1.4307, has demonstrated high ductility and strain hardening through extensive experimental evaluations, making it an ideal candidate for structural applications that require resilience under cyclic loading conditions.

This study examines the use of austenitic stainless steel EN 1.4307 as links in eccentrically braced frames (EBFs), which are a type of seismic-resistant frame. EBFs are designed to dissipate energy through shear forces in strategically placed links, making them effective in mitigating the impacts of seismic events.

The study analyzes material, element, and structural levels to comprehensively understand the performance of stainless steel in EBFs. At the material level, the focus is on the cyclic hardening behavior; at the element level, the study examines how these properties influence the links; and at the structural level, the integration of these links within EBFs is analyzed.

One significant finding is the need to revise the overstrength values for stainless steel links. Current standards do not account for the realistic overstrength of austenitic stainless steel. These revised values are essential for accurate capacity design, ensuring that EBFs perform effectively without causing non-dissipative elements to prematurely reach the plastic state. Further studies are recommended to refine these values and explore their application across different structural configurations.

1. Introduction

Stainless steel is widely recognized for its characteristics that benefit the construction industry, such as its aesthetic appearance, excellent corrosion resistance, high ductility, and superior yield strength. The latter two properties are particularly advantageous when structures are subjected to horizontal cyclic external loads. However, this relatively new material is more expensive than the commonly used carbon steel in construction.

[1] Graduate Research, Universitat Politècnica de Catalunya, Spain <lucy.laura.lazaro@upc.edu>
[2] Associate Professor, Universitat Politècnica de Catalunya, Spain, <rolando.chacon@upc.edu>

This raises the question: how can we capitalize on its advantages despite its higher cost? To address this, it is necessary to identify the types of structures that can derive the most benefits. In this research, Eccentrically Braced Frames (EBFs) were selected to analyze the application of stainless steel, aiming to propose a strategic and efficient use of this material.

There are three main types of stainless steel: austenitic, duplex, and ferritic. According to recent research (Arrayago et al. 2015) austenitic stainless steel exhibits higher ductility, while duplex stainless steel demonstrates greater strength. For the study of EBFs, higher ductility was prioritized, leading to the selection of the austenitic stainless steel type EN 1.4703.
Studies on austenitic stainless steel at the element level (Arrayago et al. 2015)(Cho et al. 2024)(Wang et al. 2024) have confirmed its higher ductility and strength. Additionally, its cyclic behavior has been tested and analyzed (Nip et al. 2010)(Zhou and Li 2016)(Jia et al. 2021). In a comprehensive study presented in recent years (Lázaro and Chacón 2022) findings on strain hardening of structural austenitic stainless steel are illustrated in Fig. 1. Noticeably, for different strain levels, there is a considerable increment of the recorded stress in cyclic tests.

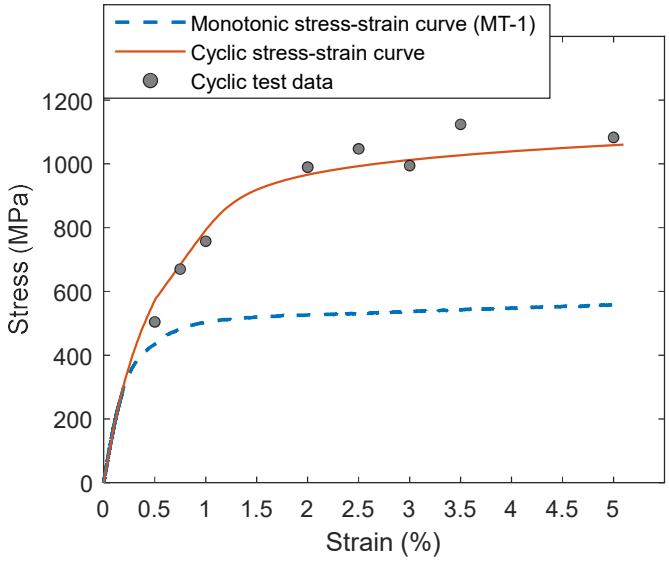

Figure 1: Monotonic and cyclic stress-strain curve of austenitic stainless steel (Lázaro and Chacón 2022)

In the same research group, findings on the cyclic behavior of austenitic stainless Steel at element levels are worth pointing out (González-de-león et al. 2022)(González-de-León et al. 2024)(Chacón et al. 2019). Moreover, tests on frames made of austenitic stainless steel subjected to incremental horizontal loads (Arrayago et al. 2020a)(Arrayago et al. 2020b) revealed greater deformations and provided insights into the pushover curves of moment-resistant frames.

This research is motivated by the strategic use of stainless steel to leverage its cyclic properties, such as higher ductility and cyclic hardening. As previously mentioned, Eccentrically Braced Frames (EBFs) were chosen for this purpose, with links made of austenitic stainless steel, while beams, braces, and columns were composed of carbon steel. This combination takes advantage of the superior energy dissipation capacity of stainless steel in the links, where plastic deformation is concentrated during seismic events. Simultaneously, the use of carbon steel for the other elements ensures cost-effectiveness and structural rigidity. This strategic material selection enhances the

overall seismic performance and resilience of the structure, making it both economical and efficient. The methodology employed in this investigation is outlined in Fig. 2.

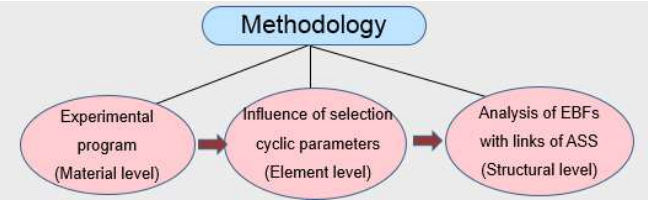

Figure 2: Methodology for the research

2. Experimental Program

The experimental program began with the design of austenitic stainless steel specimens, adhering to the following aspects: prevention of local and global buckling, compliance with ASTM E606/E606M Standards (E606/E606M. n.d.) and consideration of the testing machine – the Instron Machine (Manual n.d.). The specimen dimensions in millimeters are illustrated in Fig. 3.

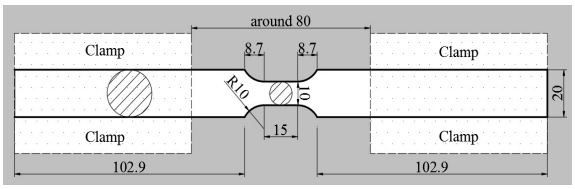

Figure 3: Design of specimens (measures are in mm)

Figure 4: Specimen manufactured

A detailed buckling analysis was performed using the finite element software Aabaqus, providing a comprehensive understanding of the structural behavior under critical loading conditions. Following this, Acerinox (steel producer) undertook the fabrication of forty designed specimens composed of austenitic stainless steel grade EN 1.4703. The finalized specimens, prepared to exact specifications, are presented in Fig. 4.

All specimens were tested at the *Laboratorio de Tecnología de Estructuras y Materiales* (LATEM) of the Polytechnic University of Catalonia, Spain. Strain gauges controlled the tests, which represented a challenge during the control of the tests. Cyclic amplitudes (response) was the source of information for defining the change of the cycle. Fig. 5 depicts the strain gauge attachment, extensometer placement for additional measurements, and the Instron Machine with specimens.

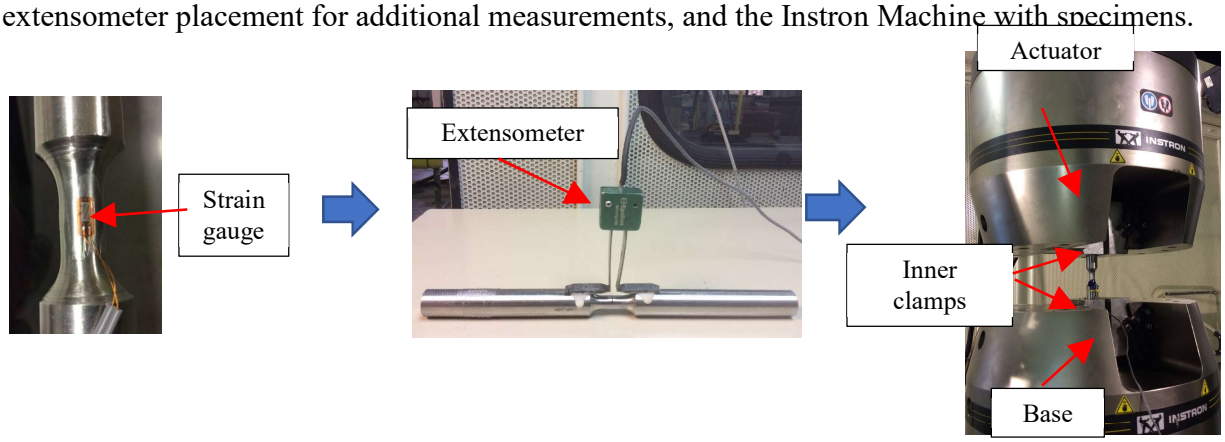

Figure 5: Strain gauge, extensometer and Instron Machine

Since strain control was employed, strain protocols guided the loading processes. Initially, an incremental monotonic strain was applied, as suggested by (Huang and Young 2014). For cyclic tests, protocols tailored to low cycle fatigue were used, applying various cyclic strain amplitudes:

1. The Companion test, designed to characterize low-cycle fatigue behavior, consisted of repeated tension and compression cycles with a constant amplitude strain.
2. The multiple-step protocol, a standard method for cases with limited specimen availability, was utilized to characterize low-cycle fatigue behavior. This approach involves a series of cycles with progressively increasing strain magnitude.
3. The Each-2-Cycles protocol, implemented in accordance with the FEMA 350 standard, involves subjecting the specimen to pairs of cycles at a constant strain amplitude before incrementally increasing the strain.
4. Special tests, designed in Barcelona, applied a constant strain amplitude as pre-strain, followed by subsequent cycles with arbitrary strain amplitudes. This approach aimed to simulate complex loading scenarios and assess material behavior under varied cyclic conditions.

Fig. 6 illustrates the strain protocol for low cyclic characterization. One end of the Instron Machine applied the strain protocols, while the other end remained fixed.

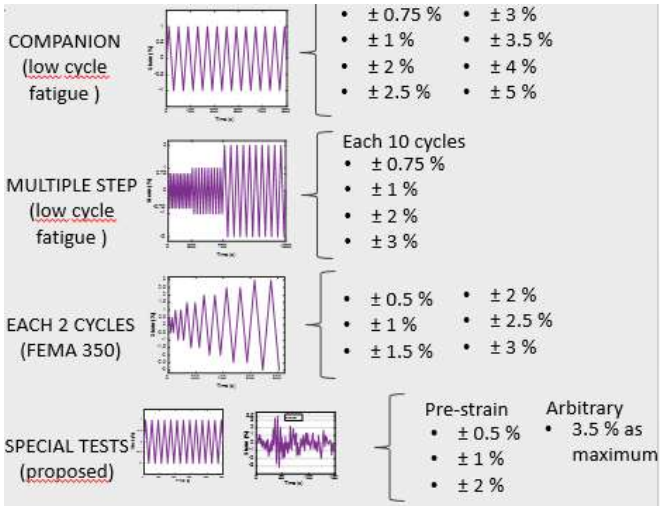

Figure 6: Loading/strain protocol for cyclic analysis

The main result from the monotonic test was a Young's Modulus of 184,152.71 N/mm². Cyclic tests produced hysteretic curves, enabling numerical model calibration for low cycle fatigue. The Chaboche model (Chaboche 2008) was employed for numerical evaluation, following the Abaqus User's Manual (Abaqus 2017). Experimental results from the Companion strain protocol of one specimen with a selected amplitude ($\pm 3\%$) is displayed in Fig. 7.

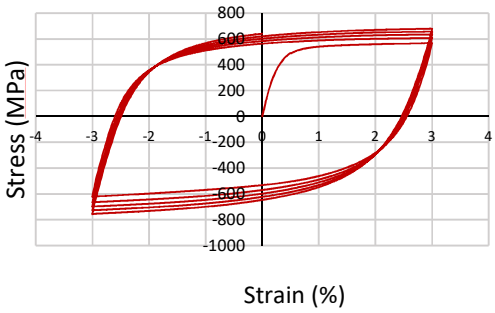

Figure 7: Experimental hysteresis curve from ±3% of strain amplitude of Companion Test

From the first to the n_{th} cycle, strain hardening is clearly observed (indicated as $\Delta\sigma$ in Fig. 8) for all experimental tests. This observation was consistently observed in all specimens. One exception worth pointing out, for the cyclic strain of $\pm 0.5\%$ was applied, the specimens showed softening instead.

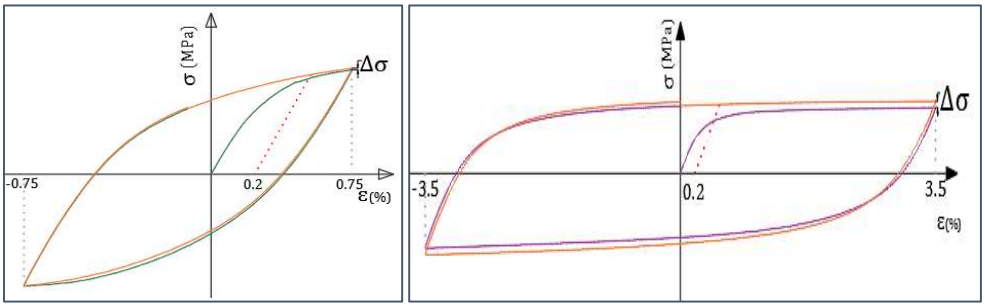

Figure 8: Cyclic strain hardening for ±0.75% and ±3.5% of strain amplitude in Companion tests

These experimental findings highlight the necessity for numerical modeling to accurately simulate and predict the observed behaviors, enabling a deeper understanding and broader applicability of the results. The Chaboche model (Chaboche 2008), which combines isotropic and kinematic hardening, was used to describe cyclic behavior.

Isotropic hardening depends on yield surface expansion (Eq. 1)

$$\sigma^0 = \sigma|_0 + Q_\infty\left(1 - e^{-b\varepsilon^p}\right) \tag{1}$$

where, $\sigma|_0$ is initial yielding stress when plastic strain equals zero, Q_∞ is the maximum change in the size of the yield surface, ε^p is plastic strain, and b is the parameter that defines the rate at which the size of the yield surface changes as plastic strain increases.

Kinematic hardening focuses on backstress movement, α. representing the midpoint stress between yield stress in tension and compression. The backstress evolution is described by Eq. 2:

$$\alpha = \frac{C_k}{\gamma_k}\left(1 - e^{-\gamma\varepsilon^p}\right) + \alpha_1 e^{-\gamma\varepsilon^p} \tag{2}$$

where C_k is the initial kinematic hardening modulus and γ_k is the rate at which the kinematic hardening modulus decreases with increasing plastic deformation. Data were obtained from the experimental results. Values for each parameter were found and provided in Table 1.

Table 1: Proposed values for cyclic behavior of austenitic stainless steel EN 1.4703

Amplitude	Combined hardening parameters				
	σ0 (MPa)	b	Q∞ (MPa)	Ck (MPa)	γk
±0.75%	367	0.48	41	81680	125
±1%	368	0.28	101	56622	307
±2.0%	334	0.78	137.05	59235	226
±2.5%	347	1.05	132	51750	215
±3%	352	1.94	127	46645	191
±3.5%	320	2.13	110	50175	181
±4%	362	5.12	63	39500	157
±5%	419	0.83	149	47692	131

Using these values, the cyclic behavior of austenitic stainless steel EN 1.4703 can be numerically characterized at the element level. This enables a detailed analysis of its mechanical response under repeated loading conditions, facilitating the development of accurate constitutive models. Such numerical characterization is crucial for predicting the material's performance in applications where cyclic loading plays a significant role, such as in seismic-resistant structures and components subjected to low cycle fatigue.

3. Influence of Cyclic Parameters

With austenitic stainless steel characterized at the element level and cyclic parameters defined, various EBFs with single-level and single-span configurations were analyzed. Fig. 9 illustrates the geometry, dimensions, and material configuration. The main objective was to understand the cyclic behavior of EBF links, focusing on element-level analysis. The material configuration consisted of austenitic stainless steel links (dissipative zones) and carbon steel braces, beams, and columns (non-dissipative elements). The numerical analysis was conducted in Abaqus and the cyclic parameters found in previous step were used (Lázaro and Chacón 2023).

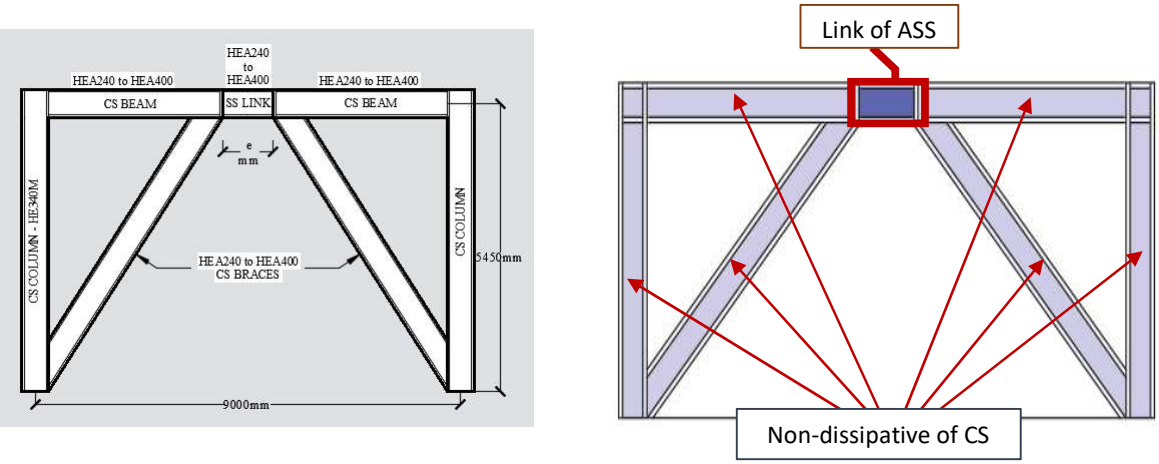

Figure 9: Geometry, measures and material configuration of simple EBFs

Monotonic analysis involved applying incremental horizontal displacement at an EBF corner to establish a displacement-strain relationship. Cyclic analysis applied horizontal displacements corresponding to 1%, 3%, and 5% strain amplitudes determined from the monotonic analysis. Fig. 10 and Table 2 detail the cyclic displacement forms and corresponding strain values.

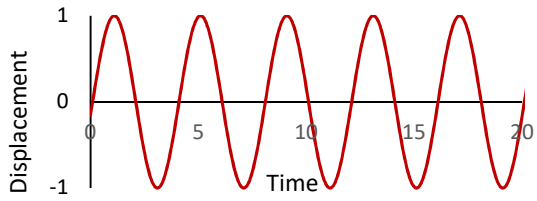

Figure 10: Form of the displacement applied

Table 2: Displacement and strain corresponding

Displacement (mm)	Strain ≈
10 to 15	1%
25 to 35	3%
40 to 60	5%

A critical question emerged regarding the selection of cyclic parameters for the analysis: which set of cyclic parameters would be most appropriate? To address this, three distinct sets of cyclic parameters were selected for evaluation.

The first set, referred to as "Single Values", corresponds to the exact strain values applied, i.e., 1%, 3%, and 5% (Table 3). The second set, referred to as "Average Values", represents the average values of all cyclic parameters found in the experimental program (Table 4). The last set, referred to as "Eight Backstresses", includes all the cyclic kinematic parameters obtained in the previous step (Table 5).

Table 3: Cyclic parameters for values of strain applied (Single values)

Strain amplitude	σ_o (N/mm^2)	Ck (N/mm^2)	γk	Q_∞	b
1%	368	56622	307	101	0.28
3%	352	46645	191	127	1.94
5%	419	47692	131	149	131

Table 4: Average values of cyclic parameters (Average values)

Material	σ_o (N/mm^2)	Ck (N/mm^2)	γk	Q_∞	b
Austenitic SS	360	53611	185	111	1.56

Table 5: All kinematic cyclic parameters (Eight backstresses)

Strain amplitude	Ck (N/mm^2)	γk	σ_o (N/mm^2)	Q_∞	b
0.75%	77270	70	360	111	1.56
1%	56622	307			
2%	59235	226			
2.5%	51750	215			
3%	46645	191			
3.5%	50175	181			
4%	39500	157			
5%	47692	131			

Thus, the parametric analysis of the EBFs was expanded to three variables, resulting in 216 numerical models.

The results were evaluated in terms of the shear angle developed by the links, the shear strength of the link, the applied displacement, and the shear at the base of the EBFs. The values found showed similarities when using the Single Values and Average Values sets. However, for the Eight Backstresses set, the results showed higher shear strength. Fig. 11 presents the results for links similar to the HEA400 profile.

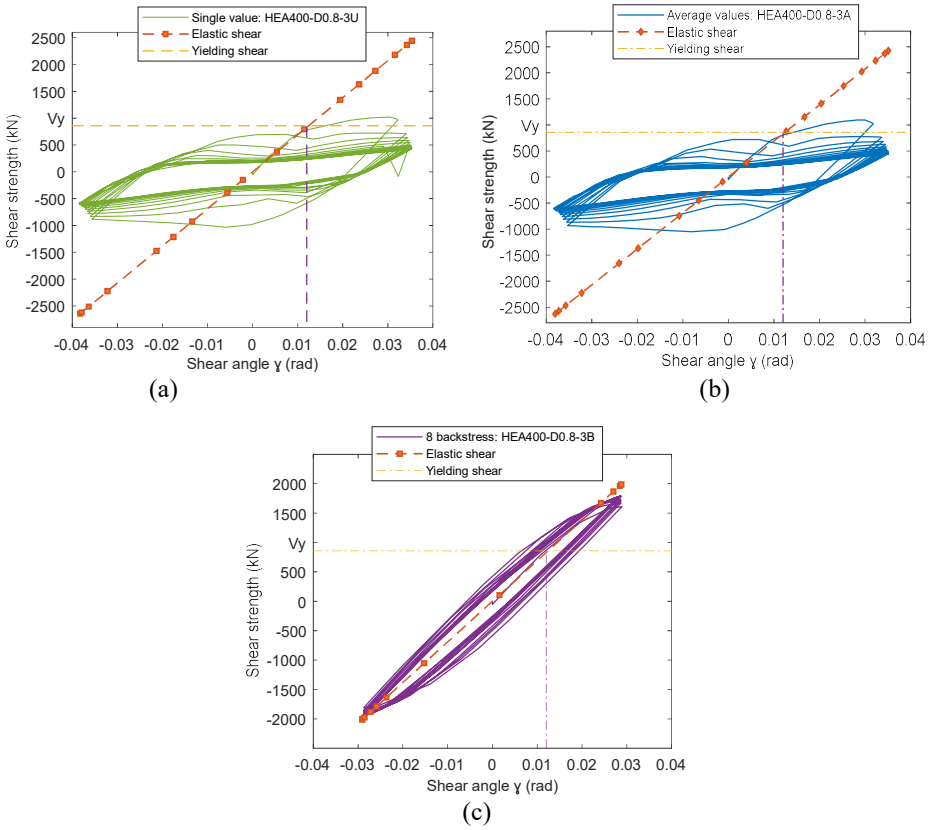

Figure 11: Shear strength of the end link for HEA400 profile

The higher strength reached with the use of Eight Backstresses led to a particular issue, where non-dissipative elements behaved as dissipative ones (Fig. 12). As shown in Fig. 12, the braces underwent deformations or reached the plastic state before the link. Therefore, the main influence of the cyclic parameter selection is illustrated by the important parameter called overstrength. Specifically, the strength of the link, which in this case was higher than that of the braces, represents an undesired behavior.

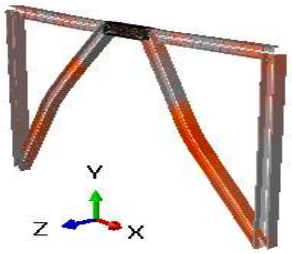

Figure 12: Failure of braces before links (HEA360 profile)

Additionally, a numerical model of the specimen used in the experimental program was created when an arbitrary load was applied. The best results were observed when the Average Values were used. Therefore, this set of cyclic parameters is recommended.

4. Overstrength Factors

In this phase, a structural-level analysis was performed. The overstrength developed by the link was considered, and the primary influence of the cyclic parameters identified in the previous step was examined. Based on these findings, several eccentrically braced frames (EBFs) were designed, featuring links made of austenitic stainless steel and non-dissipative elements (braces, beams, and columns) composed of carbon steel. Following the principles of capacity design, which require the capacity of structural elements to exceed the imposed demand, Eurocode 8 (pr EN1998-1-2:2022, 2022) specifies Eq. (3) for the design of non-dissipative elements in EBFs.

$$N_{Rd} \geq N_{Ed,G} + \gamma_{rm}\gamma_{\mathrm{sh}}\Omega_d N_{Ed,E} \tag{3}$$

where,

$\Omega_d = \min\left(\frac{V_{p,link,i}}{V_{Ed,i}}\right)$ among all short links and,

$\Omega_d = min\left(\frac{M_{p,link,i}}{M_{Ed,i}}\right)$ among all intermediate and long links,

γ_{rm} is the material overstrength factor, which is the ratio between the expected average yield strength and the nominal yield strength.

γ_{sh} stands for the strain hardening factor of the dissipative zone.

N_{Rd} represents the capacity of the element, and the other term consists of the response due to non-seismic actions and the response due to seismic actions, affected by the overstrength of the dissipative element. Consequently, Eq. 3 ensures that dissipative elements (links) achieve the plastic state first.

Nevertheless, when applying Eq. 3 to design non-dissipative elements of EBFs, the designer must select values for $\gamma_{rm} * \gamma_{sh}$. If the material used in link is austenitic stainless steel, it is necessary to use appropriate values for this material. Once again, the question arises: which value should the designer choose.

To elucidate on this conundrum, three values were proposed for analysis in this step. The first is for the case where no data is available. The second uses values derived from the analysis of the simple EBFs (previous step). The third uses values from the experimental cyclic curves.

Eurocode 8 provides values for $\gamma_{rm} * \gamma_{sh}$ for carbon steel of different grades, then these values were selected for the case where no data is available. For carbon steel S355 were selected γ_{rm} =1.25, and $\gamma_{sh} = 1.1$ as recommended by Eurocode 8. Therefore, $\gamma_{rm} * \gamma_{sh} = 1.38$.

For the second case, after analyzing the normality of the data selected from the analysis of the simple EBFs, Eq. 4 was applied, where V_{max} is the maxims shears, V_y is equal to $0.6 f_y A_V$ and $f_y = \sigma_{0.2}$.

$$\gamma_{rm} * \gamma_{sh} \cong \frac{V_{\max(Link)}}{V_{y(Link)}} \tag{4}$$

After a normality test, the cumulative probability curve was developed (Fig. 13) and was selected the 95th percentile as a probable value. Therefore $\gamma_{rm} * \gamma_{sh} = 2.45$

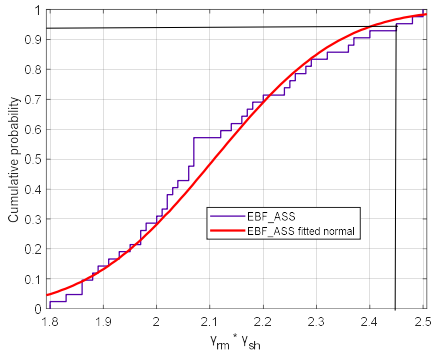

Figure 13: Cumulative probability curve for simple EBFs (previous step)

In the third case, using data from the experimental curves, the following ratios were proposed. For the strain hardening factor Eq. 5:

$$\frac{\sigma_{\max\_cyclic}}{\sigma_{0.2\ cyclic}} = 1.87 \approx \gamma_{sh} \tag{5}$$

And for the material overstrength factor Eq. 6:

$$\frac{\sigma_{0.2\ cyclic}}{\sigma_{0.2\ monotonic}} = 1.39 \approx \gamma_{rm} \tag{6}$$

where, $\sigma_{0.2\ cyclic}$, $\sigma_{0.2\ monotonic}$, $\sigma_{\max\_cyclic}$ were obtained from the Fig. 14.

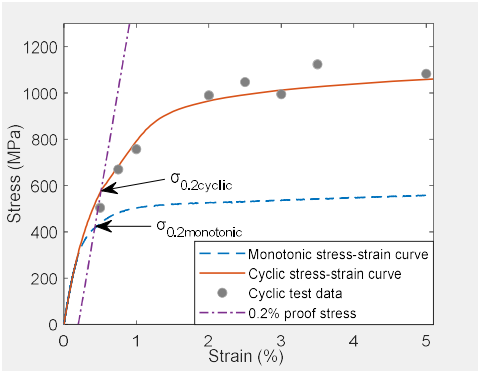

Figure 14: Cyclic and monotonic curve of austenitic stainless steel EN 1.4703

In summary, non-dissipative elements were designed using the overstrength values showen in Table 6.

Table 6: Values of overstrength proposed for analysis

Case	For carbon steel	From analysis of simple EBFs	From experimental curves
Value	$\gamma_{rm} * \gamma_{sh} = 1.38$	$\gamma_{rm} * \gamma_{sh} = 2.45$	$\gamma_{rm} * \gamma_{sh} = 2.6$

Five types of EBFs (Fig. 15) were selected for the design of non-dissipative elements using the three proposed values. Two analyses were conducted: an elastic analysis and a dynamic analysis. The elastic analysis was developed using ETABS software, while the dynamic analysis was

performed with Abaqus. A hybrid approach of beam elements for the non-dissipative zones and shell elements for the links was performed.

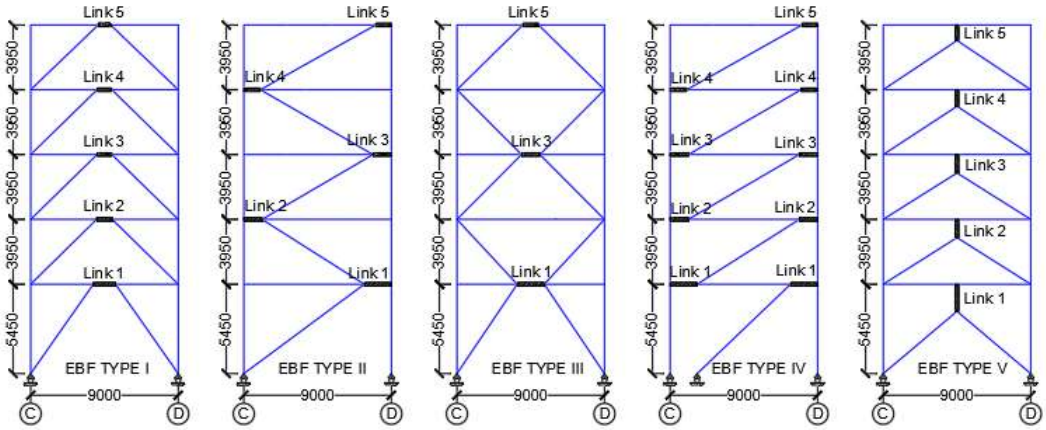

Figure 15: Five types of EBFs analyzed, configurations and measures

After the development of elastic analysis, the non-dissipative elements were designed. No resizing was required for $\gamma_{rm} * \gamma_{sh} = 1.38$. Some resizing was needed for $\gamma_{rm} * \gamma_{sh} = 2.45$, and significant resizing was suggested for $\gamma_{rm} * \gamma_{sh} = 2.6$. The latter case suggests a heavier structure and, consequently, increased costs. Fig. 16 shows the resizing requirement using colors (red means that the element requires resizeing) based on the different overstrength factors used. It is observed how different the result can be depending on this decision.

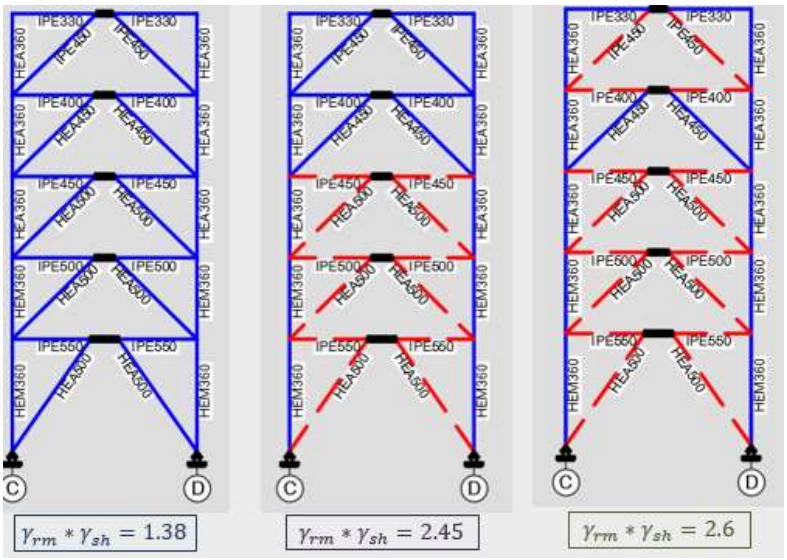

Figure 16: Design of EBF type I according different overstrength factors

It is then necessary to develop a more sophisticated analysis of the system based upon a nonlinear, time-history analysis. This dynamic analysis was performed and also suggested changes to the non-dissipative elements. For EBF Type I, resizing of the first-floor beams was suggested (Fig. 17). Therefore, an intermediate value between 1.38 and 2.45 is necessary for more realistic behavior, considering the overstrength of the link and the effective use of stainless steel.

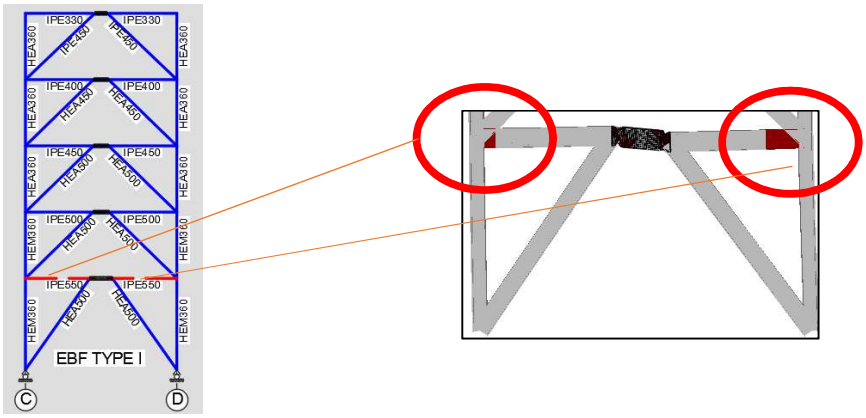

Figure 17: Suggestion of resizing of elements of EBF type I according to dynamic analysis

Based on such observations, the following equations are proposed for the overstrength factors of austenitic stainless steel. Details are provided in (Lázaro 2024).

For the strain hardening factor Eq. 7:

$$\gamma_{sh} = 1 + \frac{Q_\infty}{\sigma_o} \tag{7}$$

For $\sigma_o = 360MPa$ and $Q_\infty = 111.11MPa$ the value of $\gamma_{sh} = 1.31$

And for the material overstrength factor Eq. 6:

$$\gamma_{rm} \approx \frac{\sigma_{0.2\ cyclic}}{\sigma_{0.2\ monotonic}} \tag{8}$$

$$\gamma_{rm} = 1.39$$

Consequently a value of $\gamma_{rm} * \gamma_{sh} = 1.82$ is proposed for austenitic stainless steel links. In summary, an overstrength factor of 1.38 indicates a lack of resizing, leading to a likely failure of non-dissipative elements. Conversely, higher factors of 2.45 and 2.6 suggest excessive oversizing of the EBFs, potentially resulting in inefficient material use. The intermediate value of 1.82, however, strikes a more balanced approach, offering a realistic and practical resizing that aligns with structural performance and design efficiency. Other studies with a more systematic variation of seismic records and/or synthetic data is necessary to generalize these findings.

5. Conclusions

The strain hardening behavior exhibited by austenitic stainless steel highlights its ability to withstand significant plastic deformation while increasing its resistance under cyclic loading, making it an ideal choice for applications requiring superior cyclic performance, such as seismic-resistant structures. At the structural element level, this strain hardening directly translates into an enhanced capacity, improving the performance of eccentrically braced frames (EBFs), particularly in dissipative elements like links that play a critical role in energy dissipation during seismic events. However, achieving reliable and efficient structural designs requires accurate descriptions of overstrength factors. Underestimating overstrength may lead to the failure of non-dissipative elements, while overestimating it can result in overly conservative and inefficient designs. Striking a balance through precise estimation of overstrength is essential for ensuring both structural safety and material efficiency.

Acknowledgments
The authors acknowledge the financial support provided by the Project BIA2016-75678-R, AEI/FEDER, UE "*Comportamiento estructural de pórticos de acero inoxidable. Seguridad frente a acciones accidentales de sismo y fuego*", funded by the Spanish Ministry of Economic Affairs and Digital Transformation (MINECO). The first author acknowledges the financial support from the Peruvian Government Beca Generación del Bicentenario. The second author acknowledges SGR Ajust AGrups 2025 for the financial support.

References

ABAQUS. (2017). ABAQUS/CAE User's Manual and ABAQUS CAE Manual. Simulia Dassault Systèmes..

Arrayago, I., Real, E., & Gardner, L. (2015). Description of stress–strain curves for stainless steel alloys. Materials & Design, 87, 540–552..

Arrayago, I., González-de-León, I., Real, E., & Mirambell, E. (2020). Tests on stainless steel frames. Part I: Preliminary tests and experimental set-up. Thin-Walled Structures, 157, 107005..

Arrayago, I., González-de-León, I., Real, E., & Mirambell, E. (2020). Tests on stainless steel frames. Part II: Results and analysis. Thin-Walled Structures, 157, 107006..

Chaboche, J. L. (2008). A review of some plasticity and viscoplasticity constitutive theories. International Journal of Plasticity, 24(10), 1642–1693.

Chacón, R., Vega, A., & Mirambell, E. (2019). Numerical study on stainless steel I-shaped links on eccentrically braced frames. Journal of Constructional Steel Research, 159, 67–80.

Cho, Y., Gwon, H., Kim, K.-H., & Kim, S.-J. (2024). Static strain aging in cold rolled stable austenitic stainless steel. Journal of Materials Research and Technology, 28, 4778–4790.

E606/E606M., ASTM (2012). Standard Test Method for Stain-Controlled Fatigue Testing.

González-de-León, I., Nastri, E., Arrayago, I., Montuori, R., Piluso, V., & Real, E. (2024). Experimental programme on austenitic stainless steel RHS members subjected to monotonic and cyclic bending. Engineering Structures, 302, 117258.

González-de-León, I., Nastri, E., Arrayago, I., Montuori, R., Piluso, V., & Real, E. (2022). Experimental study on stainless steel tubular members under cyclic loading. Thin-Walled Structures, 181, 109969.

Huang, Y., & Young, B. (2014). The art of coupon tests. Journal of Constructional Steel Research, 96, 159–175.

Jia, S., Tan, Q., Ye, J., Zhu, Z., & Jiang, Z. (2021). Experiments on dynamic mechanical properties of austenitic stainless steel S30408 and S31608. Journal of Constructional Steel Research, 179, 106556.

Lázaro, L., Chacón, R. (2022). Material behaviour of austenitic stainless steel subjected to cyclic and arbitrary loading. Journal of Constructional Steel Research, 189, 107113.

Lázaro, L., & Chacón, R. (2023). Influence of the designer-assumed cyclic hardening parameters on the overstrength of austenitic stainless steel links. Thin-Walled Structures, 190, 111015.

Lázaro, L. (2024). Strategic use of austenitic stainless steel in dissipative zones of eccentrically braced frames. Doctoral Thesis. Department of Civil and Enviromental Engineering. Universitat Politècmica de Catalunya.

Manual, Reference. Instron Load Frames Reference Manual - Pre-Installatio n ©2001 Instron Corporation.

Nip, K. H., Gardner, L., Davies, C. M., & Elghazouli, A. Y. (2010). Extremely low cycle fatigue tests on structural carbon steel and stainless steel. Journal of Constructional Steel Research, 66(1), 96–110.

pr EN1998 1-2:2022. 2022. *Design of Structures for Earthquake Resistance - Part 1-2*. European Comitee for Standardisation.

Wang, Y., Hu, C., Tian, K., Li, N., Du, J., Shi, X., & Zheng, C. (2024). Excellent ductility of an austenitic stainless steel at a high strength level achieved by a simple process. Materials & Design, 239, 112796.

Zhou, F., & Li, L. (2016). Experimental study on hysteretic behavior of structural stainless steels under cyclic loading. Journal of Constructional Steel Research, 122, 94–109.